

# Vibrational resonance in bichromatically excited diatomic molecules in a shifted molecular potential

O. G. Abamba,<sup>1</sup> O. T. Kolebaje,<sup>2</sup> U. E. Vincent,<sup>1,3,\*</sup> and P. V. E. McClintock<sup>3</sup>

<sup>1</sup>*Department of Physical Sciences, Redeemer's University, Ede, Nigeria*

<sup>2</sup>*Department of Physics, Adeyemi University of Education, Ondo, 350106 Nigeria*

<sup>3</sup>*Department of Physics, Lancaster University, Lancaster LA1 4YB, United Kingdom*

(Dated: August 27, 2024)

For bichromatically excited diatomic molecules modelled in a shifted Tietz-Wei molecular potential, we demonstrate the occurrence of vibrational resonance (VR) when a saddle-node (SN)-bifurcation takes place, and its non-occurrence in the absence of an SN-bifurcation. We have examined the VR phenomenon and its connection with SN-bifurcation for eight diatomic molecules, namely, H<sub>2</sub>, N<sub>2</sub>, Cl<sub>2</sub>, I<sub>2</sub>, O<sub>2</sub>, HF, CO, and NO, consisting of homogeneous, heterogeneous and halogen molecules. We demonstrate that each of them vibrates at a distinct resonant frequency but with a spread in frequency. The high-frequency amplitude at which VR occurs corresponds to the SN-bifurcation point. We validate our analytic results by numerical simulations, and show that the homonuclear halogens respond only weakly to bichromatic fields, which may perhaps be linked to their absence of SN-bifurcation.

Keywords: Vibrational Resonance, biharmonics, diatomic molecules, shifted Tietz-Wei potential, molecular vibration.

## I. INTRODUCTION

Interest in the effect of bichromatic excitation on the dynamics of nonlinear systems, and an appreciation of its importance, dates back to the 1970s when Ambartzumlan and Letokhov reported [1] that the dissociation of polyatomic molecules may more easily be achieved by using a biharmonic (rather than a monochromatic) infrared laser field. Since then, there has been remarkable growth in theoretical and experimental investigation of bichromatic fields across physics, biology, chemistry, and other areas of science [2–11]. Many of the earlier studies focused on coherent control of the molecular dynamics based on the nonlinear theory of classical conservative systems [2–5]; a few considered dissipative systems [6, 7]. Recently, however, the latter have received renewed interest due to the rich and fascinating dynamical properties arising from the interplay between the frequency components. These properties are distinct from those displayed by the corresponding conservative systems.

The most frequently observed and investigated phenomena in bichromatically driven dissipative systems relate to their nontrivial complex dynamics, and include *quasiperiodicity* and *strange nonchaotic attractors* [12], *bursting, i.e. mixed-mode oscillations* [13–15], *synchronization, i.e. phase-locked states*, and *resonances* [16–18]. Although ubiquitous in many natural and technological systems and with a range of potential applications, these phenomena and the mechanisms underlying them are not fully understood, either theoretically or experimentally, despite much effort [17–20]. In particular, the diverse manifestation of resonances in mechanical, electrical, acoustic, biological, quantum, and molecular sys-

tems makes resonance oscillations increasingly appealing for exploitation in a wide range of investigations [17–21]. In molecular systems, when two slow atoms interact such that there is matching between a bound state energy in the interatomic potential, and the excitation/vibrational energy of the atoms, a resonance phenomenon known as vibrational Feshbach resonance (VFR) occurs [22, 23]. Since its discovery, VFR has been reported in numerous molecular systems [23]. VFR is now well established as the mechanism underlying positron annihilation polyatomic molecules [23–26]. In this paper, we report on a different kind of vibrational resonance (VR) in molecular systems which may arise when they are driven by bichromatic frequency fields. This form of VR phenomenon and its potential applications have recently been classified and enumerated [18–20, 27]. It encompasses: the detection, amplification and transmission of very weak signals; diagnosis of faults in bearings and rotating machinery; the harvesting of electrical energy from environmental vibrations; the operation of memory devices such as set-reset logic gates; and nano-electromechanical resonators [15, 18–20]. In addition, experimental applications to a thermo-optic optomechanical nanocavity [28] and to an optoelectronic artificial spiking neuron [29] have been reported very recently.

In VR, the response of a non-linear system to the effect of the lower-frequency ( $L_f$ ) component of the bichromatic excitation can be amplified by the presence of the high-frequency ( $H_f$ ) component when the difference between the two frequencies is sufficiently large [16]. Landa and McClintock [16] reported the VR phenomenon in 2000, linking it to *stochastic resonance* (SR) – a noise-induced resonance, in which stochastic excitation amplifies the output of a weak signal [30, 31]. Following the theoretical validation of VR by Gitterman and others [32, 33]), there have also been several experimental investigations of the effect [28, 29, 34–38].

---

\* Corresponding author: u.vincent@lancaster.ac.uk

In what follows, we investigate VR in a classical dissipative oscillator akin to that used by Knop and Lauterborn [39], Jing *et al.* [40] and Abirami *et al.* [41] to model interatomic potentials. Such oscillators can be used to describe the molecular dynamics at moderate and high rotational and vibrational quantum numbers [42]. Notably, however, they have been neglected in the study of VR, despite their applications in molecular physics and mechanics, as well as in chemistry and material science, for elucidating molecular properties, and especially those of diatomic molecules. Several suitable interatomic potentials have been proposed for this purpose. The first of these, and the one most conventionally used for diatomic molecules, was the Morse potential (MP) [43] investigated for VR by Abirami *et al.* [17, 41]. In addition to the MP, many other interatomic potential energy representations have also been proposed for diatomic molecules [44]. These variants and, in particular, their shifted forms with multi-parameters, offer possible advantages over the MP. For instance, the shifted Tietz-Hua (sTH), proposed by Falaye *et al.* [45]), also known as the shifted Tietz-Wei (sTW), essentially represents the Tietz-Wei (TW) potential [42, 46, 47], shifted by the dissociation energy,  $V_0$ . Its energy spectrum for diatomic molecules shows better agreement than either the MP or the TW potential for arbitrary quantum numbers. This advantage is attributable to its multi-parameter properties. Unsurprisingly, interatomic potentials with a larger number of parameters tend to fit experimental data better [48, 49].

Motivated by these considerations, there have been several studies based on the sTW potential system, some of which are described in Refs. [50–57]. Here, we investigate and report the occurrence of VR phenomena in the sTW potential under the influence of a biharmonic signal. We focus on the following diatomic molecules for which experimental values of the  $c_h$  parameter (see table I) in the sTW potential exist:  $N_2$ ,  $O_2$ ,  $NO$ ,  $CO$ ,  $I_2$ ,  $H_2$ ,  $Cl_2$  and  $HF$ . Each consists of two covalently bonded atoms, of either identical or nonidentical chemical species [58]. Diatomic molecules are, of course, very commonly encountered in natural and industrial processes, such as combustion, atmospheric chemistry, nuclear water reactors, and laser spectroscopy. This makes them a subject of significant scientific interest [59, 60]. We will show that the amplitude of the fast excitation for which VR arises corresponds to a saddle-node (SN-) bifurcation parameter value, and that a molecule will vibrate at a distinct resonant frequency corresponding to the SN-bifurcation, with a broadened frequency width. Furthermore, we show that, in general, the homogeneous halogens, do not undergo an SN-bifurcation or any known bifurcation in the fast oscillation parameter space investigated. Consequently, they respond only weakly to bichromatic fields. This behaviour could be attributed to their relatively heavy masses compared to those of the non-halogen and heterogeneous halogen diatomic molecules studied as well as other chemical properties peculiar to them. Our theoretical analysis of these phenomena, based on the method

of the separation of time scales, has been validated by numerical simulations of the equations. .

The paper is structured as follows: In section II, we present the model equation. In section III, a theoretical analysis of VR is carried out. In section IV, the numerical simulation results and our findings are discussed. In section V, we summarize and conclude the paper.

## II. MODEL

We examine the classical motion of a bichromatically excited oscillator in a model interatomic potential. The dissipative nonlinear dynamics of the system may be written in terms of inter-nuclear distance ( $r$ ) as [39–41]

$$\ddot{r} + \delta\dot{r} + \frac{dV(r)}{dr} = F \cos \omega t + G \cos \Omega t. \quad (1)$$

Here, the time-periodic functions,  $F \cos \omega t$  and  $G \cos \Omega t$  are respectively the low-frequency ( $L_F$ ) and high-frequency ( $H_F$ ) components of the bichromatic excitation,  $d$  is the dissipation coefficient,  $F$  is the amplitude of the slow excitation component of frequency  $\omega$ ,  $G$  is the amplitude of the fast excitation component of frequency  $\Omega$ , and  $V(r)$  is the shifted Tietz-Wei (sTW) potential. In practice, the two frequency fields, may arise from a combination of Aharonov-Bohm and magnetic flux fields [61–64] or electromagnetic fields [61, 65–67] – all which can impact on the quantum levels as well as on the vibrational energy states, as demonstrated by Falaye *et al.* [62] for a hydrogen atom in a quantum plasma through cooperation between a strong electric field and a weak magnetic field [62].

The sTW potential model integrates the effects of anharmonicity and other nonidealities. It is characterized by four parameters: the parameter trio of angular frequency  $\omega_e$ , equilibrium bond length  $r_e$ , and dissociation energy  $V_0$ ; plus an additional adjustable parameter  $c_h$ . This latter was introduced to reduce the difference between calculated values and those obtained *ab initio* or from Rydberg-Klein-Rees (RKR) potentials [56, 57]. The sTW potential is written as

$$V(r) = V_0 \left( \frac{Ae^{-b_h(r-r_e)} - Be^{-2b_h(r-r_e)}}{(1 - c_h e^{-b_h(r-r_e)})^2} \right), \quad (2)$$

where  $A = 2(c_h - 1)$ ,  $B = (c_h^2 - 1)$ ,  $c_h$  is the optimization parameter,  $b_h = \gamma(1 - c_h)$ ,  $V_0$  is the dissociation energy,  $r_e$  is the molecular bond length, and  $\gamma$  is the Morse constant, defined as  $\gamma = \omega_e \sqrt{2\pi^2 \frac{c^2 \mu}{V_0}}$ , with  $\mu$  being the reduced molecular mass. The sTW potential is similar to the Morse potential when  $c_h = 0$ , but differs when  $c_h \neq 0$ . This difference enables the STW potential to simulate atomic interactions more effectively than the conventional Morse potential [45].

The shape of the sTW potential is shown in Fig. 1 for the different diatomic molecules investigated in this

paper, namely, H<sub>2</sub>, O<sub>2</sub>, HF, Cl<sub>2</sub>, I<sub>2</sub>, CO, NO, and N<sub>2</sub>. The values of the spectroscopic parameters used are given in table I.

### III. THEORETICAL ANALYSIS

Inserting Eq. (2) into Eq. (1), it is straightforward to show that the system to be analysed becomes

$$\begin{aligned} \ddot{r} + \delta\dot{r} - V_0 b_h \left( A e^{-b_h(r-r_e)} + 4A c_h e^{-2b_h(r-r_e)} \right. \\ \left. - 2B e^{-2b_h(r-r_e)} + 9A c_h^2 e^{-3b_h(r-r_e)} - 6B c_h e^{-3b_h(r-r_e)} \right. \\ \left. + 6A c_h^3 e^{-4b_h(r-r_e)} - 12B c_h^2 e^{-4b_h(r-r_e)} \right) \\ = F \cos \omega t + G \cos \Omega t. \end{aligned} \quad (3)$$

To solve this equation, we employed the method of separation of time scales, thus separating the solution for the inter-nuclear distance  $r(t)$  into two parts related to the slow and fast motions respectively. Because  $\Omega \gg \omega$ , we assume that the solution of Eq. (3) is of the form:

$$r(t) = \chi(t) + \psi(t, \tau), \quad \text{where } t = \frac{2\pi}{\omega} \text{ and } \tau = \Omega t. \quad (4)$$

Here  $\chi$  and  $\psi$  are respectively the slow motion variable with frequency  $\omega$  and period  $\frac{2\pi}{\omega}$ , and the fast motion variable in fast time  $\tau$  with frequency  $\Omega$  and period  $\frac{2\pi}{\Omega}$ . Substituting Eq. (4) into Eq. (3), we obtain the equation for the slow motion as:

$$\begin{aligned} \ddot{\chi} + \delta\dot{\chi} - V_0 b_h \left( A e^{-b_h(\chi-r_e)} \langle e^{-b_h\psi} \rangle \right. \\ \left. + (4A c_h - 2B) e^{-2b_h(\chi-r_e)} \langle e^{-2b_h\psi} \rangle \right. \\ \left. + (9A c_h^2 - 6B c_h) e^{-3b_h(\chi-r_e)} \langle e^{-3b_h\psi} \rangle \right) \\ = F \cos(\omega t), \end{aligned} \quad (5)$$

and that for the fast motion component as:

$$\begin{aligned} \ddot{\psi} + \delta\dot{\psi} - V_0 b_h \left( A e^{-b_h(\chi-r_e)} (e^{-b_h\psi} - \langle e^{-b_h\psi} \rangle) \right. \\ \left. + (4A c_h - 2B) e^{-2b_h(\chi-r_e)} (e^{-2b_h\psi} - \langle e^{-2b_h\psi} \rangle) \right. \\ \left. + (9A c_h^2 - 6B c_h) e^{-3b_h(\chi-r_e)} (e^{-3b_h\psi} - \langle e^{-3b_h\psi} \rangle) + \Gamma_1 \right) \\ = G \cos(\Omega t), \end{aligned} \quad (6)$$

where

$$\Gamma_1 = (6A c_h^3 - 12B c_h^2) e^{-4b_h(\chi-r_e)} (e^{-4b_h\psi} - \langle e^{-4b_h\psi} \rangle).$$

Since  $\psi$  is a rapidly changing function of time  $\tau$  then, by employing the inertial approximation  $\dot{\psi} \gg \ddot{\psi} \gg \psi$ , we can approximate Eq. (6) as  $\ddot{\psi} = g \cos(\Omega t)$ ,  $\dot{\psi} =$

TABLE I. Spectroscopic parameter values for diatomic molecules modelled by the shifted Tietz-Wei molecular potential [68–73]

Molecule	$\mu$ (u)	$r_e$ (Å)	$V_0$ (eV)	$b_h$ (Å <sup>-1</sup> )	$c_h$
N <sub>2</sub>	7.0034	1.0940	9.90	2.7859	-0.0323
NO	7.5215	1.1508	8.044	2.7156	0.0137
CO	6.8607	1.1283	10.845	2.2048	0.1499
O <sub>2</sub>	7.9975	1.208	5.1567	2.5910	0.0273
I <sub>2</sub>	63.4522	2.662	1.5818	2.1234	-0.1390
H <sub>2</sub>	0.5039	0.7416	4.7446	1.6189	0.1701
Cl <sub>2</sub>	17.6083	1.987	2.5139	2.2035	-0.0970
HF	9.5014	0.917	6.120	1.9421	0.1278

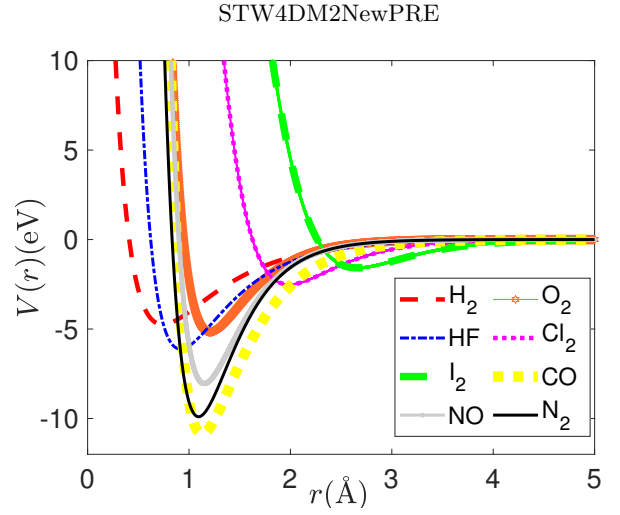


FIG. 1. The shape of shifted Tietz-Wei molecular potential for different diatomic molecules.

$\frac{g}{\Omega} \sin(\Omega t)$ , and  $\psi = \frac{g}{\Omega^2} \cos(\Omega t)$ . Let  $\zeta = \frac{g}{\Omega^2}$ . Then  $\dot{\psi} = -\zeta \cos(\Omega t)$ , and the following time averages apply:  $\langle e^{-b_h\psi} \rangle = I(b_h\zeta) = I_1$ ,  $\langle e^{-2b_h\psi} \rangle = I(2b_h\zeta) = I_2$ ,  $\langle e^{-3b_h\psi} \rangle = I(3b_h\zeta) = I_3$ , and  $\langle e^{-4b_h\psi} \rangle = I(4b_h\zeta) = I_4$ , where  $I_1, I_2, I_3$  and  $I_4$  are zeroth-order modified Bessel functions of the first kind. Use of the time averages allows us to simplify Eq. (5), so that the equation for the slow motion becomes

$$\begin{aligned} \ddot{\chi} + \delta\dot{\chi} - V_0 b_h \left( A e^{-b_h(\chi-r_e)} I_1 \right. \\ \left. + (4A c_h - 2B) e^{-2b_h(\chi-r_e)} I_2 \right. \\ \left. + (9A c_h^2 - 6B c_h) e^{-3b_h(\chi-r_e)} I_3 + \Gamma_1 \right) \\ = F \cos(\omega t), \end{aligned} \quad (7)$$

where  $\Gamma = (6A c_h^3 - 12B c_h^2) e^{-4b_h(\chi-r_e)} I_4$ . The effective

potential,  $V_{eff}$  of the oscillator Eq. (7) then becomes:

$$V_{eff}(\chi) = V_0 \left( \alpha_1 I_1 e^{-b_h(\chi-r_e)} + \frac{\alpha_2 I_2}{2} e^{-2b_h(\chi-r_e)} + \frac{\alpha_3 I_3}{3} e^{-3b_h(\chi-r_e)} + \frac{\alpha_4 I_4}{4} e^{-4b_h(\chi-r_e)} \right), \quad (8)$$

where  $A = \alpha_1$ ,  $(4Ac_h - 2B) = \alpha_2$ ,  $(9Ac_h^2 - 6Bc_h) = \alpha_3$ , and  $(6Ac_h^3 - 12Bc_h^2) = \alpha_4$ .

Irrespective of the system parameters,  $V_{eff}(\chi)$  is always a single well with a minimum located at  $\chi_x = r_e - \frac{1}{b_h} \ell_n k$ , where  $e^{-b_h(\chi_x-r_e)} = k$  and  $b_h(r_e - \chi_x) = \ell_n k$ . The deviation from the minimum  $Y = \chi - \chi_x$  is given by

$$\ddot{Y} + \delta \dot{Y} - V_0 b_h \left( \alpha_1 I_1 e^{-b_h Y} e^{-b_h(\chi_x-r_e)} + \alpha_2 I_2 e^{-2b_h Y} e^{-2b_h(\chi_x-r_e)} + \alpha_3 I_3 e^{-3b_h Y} e^{-3b_h(\chi_x-r_e)} + \alpha_4 I_4 e^{-4b_h Y} e^{-4b_h(\chi_x-r_e)} \right) = F \cos(\omega t). \quad (9)$$

By expansion,  $e^{-b_h Y} \approx 1 - b_h Y$ ,  $e^{-2b_h Y} \approx 1 - 2b_h Y$ ,  $e^{-3b_h Y} \approx 1 - 3b_h Y$ , and  $e^{-4b_h Y} \approx 1 - 4b_h Y$ . Thus, Eq. (9) becomes:

$$\ddot{Y} + \delta \dot{Y} + V_0 \left( \alpha_2 I_2 k^2 b_h^2 + 2\alpha_3 I_3 k^3 b_h^2 + 3\alpha_4 I_4 k^4 b_h^2 \right) Y = F \cos(\omega t), \quad (10)$$

which can be rewritten as,

$$\ddot{Y} + \delta \dot{Y} + \omega_r^2 Y = F \cos(\omega t), \quad (11)$$

where

$$\omega_r^2 = V_0 \left( \alpha_2 I_2 k^2 b_h^2 + 2\alpha_3 I_3 k^3 b_h^2 + 3\alpha_4 I_4 k^4 b_h^2 \right),$$

and  $\omega_r$  is the natural resonant frequency of the oscillator in its stable state.

To obtain the theoretical expression for the response  $Q$  of the slow motion of the oscillator to high frequency excitation, we solve the linear differential Eq. 11 by the differential operator method. This yields, the solution for  $Y$  as

$$Y \equiv A \cos(\omega t) + B \sin(\omega t) = R_L \cos(\omega t + \theta), \quad (12)$$

where  $A = \frac{(\omega_r^2 - \omega^2)F}{(\omega_r^2 - \omega^2)^2 + d^2\omega^2}$ ,  $B = \frac{dF\omega}{(\omega_r^2 - \omega^2)^2 + d^2\omega^2}$ , and  $\theta$  is the phase angle of the oscillator. Then, by defining  $R_L^2 = A^2 + B^2$ , one can show that

$$R_L = \frac{F}{\sqrt{(\omega_r^2 - \omega^2)^2 + d^2\omega^2}}. \quad (13)$$

Thus, the analytic response amplitude,  $Q$  at the frequency  $F$  of the weak excitation is given by

$$Q = \frac{R_L}{F} = \frac{1}{\sqrt{(\omega_r^2 - \omega^2)^2 + d^2\omega^2}}. \quad (14)$$

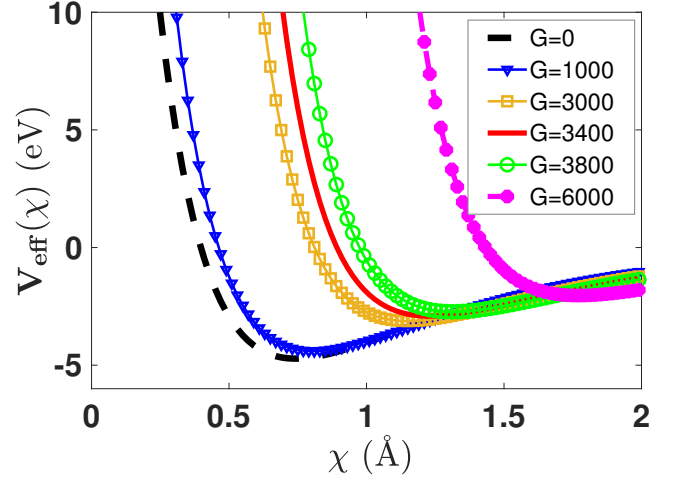


FIG. 2. The effective potential  $V_{eff}(\chi)$  of the bi-harmonic system of equation (8) for the  $H_2$  diatomic molecule, with  $\Omega = 70$ ,  $\omega = \sqrt{20}$ , and  $f = 0.1$ , with other parameters of the molecule as shown in Table I, for different amplitudes of the fast excitation amplitude  $G = 0, 1000, 3000, 3400, 3800$  and  $6000$ . The shape of the potential and its well depth can be seen to depend on the high-frequency amplitude  $G$ .

#### IV. NUMERICAL SIMULATION

We now describe the numerical procedures used and then report the results obtained, comparing them with the analytic results of Sec. III.

##### A. Numerical procedures

To solve Eq. (3) numerically, we transform it into the equivalent system of two first-order ODEs:

$$\begin{aligned} \frac{dx}{dt} &= Y \\ \frac{dy}{dt} &= V_0 b_h \left( A e^{-b_h(r-r_e)} + 4Ac_h e^{-2b_h(r-r_e)} - 2B e^{-2b_h(r-r_e)} \right. \\ &\quad + 9Ac_h^2 e^{-3b_h(r-r_e)} - 6Bc_h e^{-3b_h(r-r_e)} \\ &\quad + 6Ac_h^3 e^{-4b_h(r-r_e)} - 12Bc_h^2 e^{-4b_h(r-r_e)} \left. \right) \\ &\quad - \delta y + F \cos \omega t + G \cos \Omega t. \end{aligned} \quad (15)$$

Equation (15) was solved numerically using the Simulink platform – a MATLAB add-on product – modeling and simulating the components of the system as shown in Fig. 17 [74].

Table I presents details of the spectroscopic parameters of the diatomic molecules used in the simulation. Unless otherwise specified, the following parameters remained fixed:  $\delta = 0.1$ ,  $\Omega = 70.0$ ,  $\omega = \sqrt{20}$ ,  $F = 0.1$ , and time step of the simulation was  $\frac{T}{200}$ . To calculate the response

to the external excitation, we note that any periodic function can be expressed as the sum of its Fourier components, where  $T = \frac{2\pi}{\omega}$  represents the period of oscillation of the low-frequency force  $L_F$ . Thus, we computed the system's response amplitude  $Q$  at the frequency of the slow excitation from the output signal's Fourier spectrum in the usual form:

$$Q = \frac{\sqrt{Q_S^2 + Q_C^2}}{F}, \quad (16)$$

where  $Q_S$  and  $Q_C$  are the Fourier sine and cosine components of the time series of the output signal  $r(t)$ , respectively, and are expressed as

$$Q_S = \frac{2}{nT} \int_0^{nT} r(t) \sin \omega t dt, \quad (17)$$

$$Q_C = \frac{2}{nT} \int_0^{nT} r(t) \cos \omega t dt. \quad (18)$$

The numerical integration was performed over the time interval of  $nT$ , where  $n = 1, 2, 3, \dots$  is the number of complete oscillations.

## B. Frequency response

Figure 3 shows the frequency-response curve, illustrating the dependence of  $Q$  on the frequency  $\omega$  of the slow excitation for different amplitudes of the fast excitation component of the bichromatic drive. The parameters used are those of the  $H_2$  molecule and  $Q$  was calculated for four different values of  $G$  — the amplitude of the fast component ( $G = 0, 1000, 3000$ , and  $6000$ ). At  $G = 0$ , the fast excitation is absent. The primary resonance then occurs at the resonant frequency  $\omega_0 = 5.9$ . With increasing values of  $G$ , the response  $Q$  grows near  $\omega_0$  but experiences a sudden discontinuous jump at  $\omega_0$ , with a peaks ranging from 1.1 for  $G = 0$  to 1.8 for  $G = 6000$ . Discontinuous resonance jumps are often connected with dynamical hysteresis in which a system jumps between coexisting attractors in an irreversible fashion as a system parameter is varied forward and backward [75–79]. Notably, the resonance peaks occur in the frequency range  $3.0 \leq \omega \leq 7.0$ . The amplification is accompanied by shifts in the resonance frequency ( $\omega_0$ ) to lower  $\omega_0$  values: when  $G = 1000$ ,  $\omega_0 = 5.6$ ;  $G = 3000$ ,  $\omega_0 = 4.7$ ; and at  $G = 6000$ ,  $\omega_0 = 3.8$ . There is reasonable agreement between the numerical and the analytical response curves.

Next, we examine the dependence of  $Q$  on the frequency ( $\Omega$ ) of the fast signal, while setting its amplitude to  $G = 0, 1000, 3000$ , and  $6000$  for an  $H_2$  molecule. From Fig. 4 we observe that, as the value of  $G$  is increased, the  $H_f$  frequency bandwidth increases proportionally. In the absence of high frequency forcing, i.e. at  $G = 0$ , the  $H_f$  frequency bandwidth is narrower. For the  $H_f$  amplitude

of  $G = 3000$ ,  $Q$  peaks within the range  $91.5 \geq \Omega \geq 97.5$ . Notably, at  $G = 6000$ ,  $Q$  peak occurs within the range  $97.5 \geq \Omega \geq 105$ . Again, the jump phenomenon appears. In this case, however,  $Q$  grows and attains its peak, then suddenly drops. Thus, the parameters of the high-frequency component of the excitation can be tuned, appropriately, to achieve the desired frequency-response or to avoid some frequency range.

We also examined the response curve when the system is controlled by the slow component of the excitation (at frequency  $\omega$ ), as shown in Fig. 5. It can be seen that the width of the system's response  $Q$  broadens substantially as  $\omega^2$  decreases. However, the height of the resonance peak remains unaltered. Evidently, as the value of  $\omega^2$  increases, the width of the resonance curve decreases. However, as  $\omega^2$  increases, the value of  $G$  at which the resonance occurs shifts to the left. For  $\omega^2 = 10, 15$ , and  $20$ , the peak occurred at  $3400, 6000$ , and  $10,000$ , respectively. These numerically computed resonance curves are in satisfactory agreement with those calculated analytically from Eq. (14). Again, the parameters of the potential correspond to those of an  $H_2$  molecule

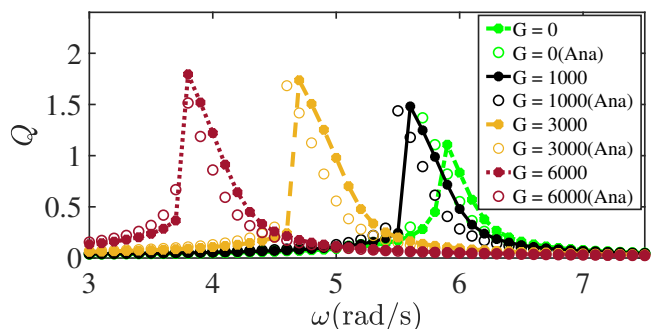


FIG. 3. The frequency-response curve, showing the dependence of response amplitude  $Q$  on the slow excitation frequency  $\omega$  for  $\Omega = 70.0$ ,  $\delta = 0.1$ ,  $F = 0.1$ , and for  $G = 0, 1000, 3000$ , and  $6000$ , using the parameters for the  $H_2$  diatomic molecule given in table I). The continuous line represents the numerically computed  $Q$  from Eq. (15) using Eq. (16), while the markers represent the corresponding analytic solution given by Eq. (14).

## C. VR for diatomic molecules

In the preceding discussion, we established the occurrence of VR in diatomic molecules, using the  $H_2$  molecule as an example. We now proceed to examine the responses to fast excitations of each of the eight examples of diatomic molecules proposed for investigation:  $O_2$ ,  $N_2$ ,  $H_2$ ,  $CO$ ,  $HF$ ,  $Cl_2$ ,  $I_2$  and  $NO$ . In doing so, we hope to unravel the features specific to each molecule and to each molecular group. The values of the spectroscopic parameters used for each molecule are given in Table I. It is well known that quantized vibrational modes arise in

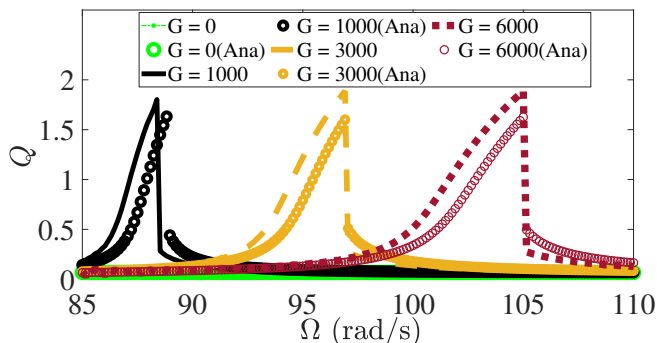


FIG. 4. The frequency-response curve,  $Q$  vs.  $\Omega$ , the frequency of the fast excitation, for different values of its amplitude  $G = 0, 1000, 3000$ , and  $6000$ , for  $\delta = 0.1$ ,  $F = 0.1$ , and  $\omega = \sqrt{20}$ , for an  $\text{H}_2$  diatomic molecule with the parameter values given in table 1. The continuous curves represent the numerically computed  $Q$  from Eq. (15) using Eq. (16), while the analytical solutions obtained from Eq. (14), are indicated by markers.

homonuclear diatomic molecules, such as hydrogen ( $\text{H}_2$ ), oxygen ( $\text{O}_2$ ), and nitrogen ( $\text{N}_2$ ), due to the symmetrical bonding between identical atoms [80]. The two homogenous halogens: iodine ( $\text{I}_2$ ) and chlorine ( $\text{Cl}_2$ ) are also homonuclear diatomic molecules. In contrast, heteronuclear diatomic compounds, such as carbon monoxide ( $\text{CO}$ ), nitric oxide ( $\text{NO}$ ), and hydrogen fluoride ( $\text{HF}$ ), exhibit complex vibrational landscapes due to the different masses and electro-negativities of the pairs of atoms forming each molecule [80].

We begin by considering the low frequency responses plotted in Fig. 6, which shows results for all eight diatomic molecules. It illustrates the dependence of  $Q$  on the slow excitation frequency  $\omega$  keeping the amplitude of the fast excitation fixed at  $G = 0$  (upper panel, with no high frequency excitation) or  $G = 12,000$  (lower panel), respectively. Comparing the two panels, we can see that each molecule vibrates at a different resonant frequency as the fast excitation is turned off or on. The primary resonances ( $\omega_0$ ) of the eight diatomic molecules differ. We obtained a numerical value of the resonance frequency for each of them: for  $\text{H}_2$ ,  $\omega_0 = 8.35$ ; for  $\text{I}_2$ ,  $\omega_0 = 4.9$ ; for  $\text{Cl}_2$ ,  $\omega_0 = 6.1$ ; for  $\text{HF}$ ,  $\omega_0 = 11.05$ ; for  $\text{O}_2$ ,  $\omega_0 = 12.1$ ; for  $\text{NO}$ ,  $\omega_0 = 11.35$ ; for  $\text{N}_2$ ,  $\omega_0 = 12.7$ ; and for  $\text{CO}$ ,  $\omega_0 = 12.85$ . When the high frequency forcing is switched on (lower panel), the resonant frequencies for  $\text{H}_2$ ,  $\text{I}_2$ ,  $\text{Cl}_2$ ,  $\text{HF}$ ,  $\text{O}_2$ ,  $\text{NO}$ ,  $\text{N}_2$ , and  $\text{CO}$  change to 4.15, 1.9, 2.65, 5.2, 5.35, 2.35, 2.95, and 3.55, respectively. The analytic response curves agree reasonably well with the numerical simulations.

Figure 7, shows the response amplitude  $Q$  plotted against the amplitude  $G$  of the high frequency force for each of the molecules. There is a distinct and well-defined resonance peak for each of the non-halogens and non-homonuclear halogens; in contrast, each of the homonuclear halogens oscillates minimally in its quiescent mode without exhibiting a resonance. One possible inference could be that VR depends on the molecular mass (See

Table I). The  $\text{H}_2$  molecule, which is the lightest, with a mass of 2 u, exhibits the highest response peak, occurring in the neighbourhood of  $G = 0.5$  and the narrowest resonance width – a signature of a well-defined and stable vibrational state with slower transitions [80]. Weak responses were observed for the  $\text{Cl}_2$  and  $\text{I}_2$  molecules, which have atomic masses of 71 u and 135 u, respectively. These two molecules are the heaviest among those investigated, and they belong to halogen group in the periodic table. Their relatively weak responses to the high frequency excitation probably relate to their higher masses relative to the non-halogen molecules examined:  $\text{CO}$ ,  $\text{N}_2$ , and  $\text{NO}$  have moderate atomic masses of 28 u, 28 u, and 30 u, respectively, and relatively high dissociation energies relative to the other molecules. For these molecules, resonances occur at high values of  $G$  with approximately equal peak heights. In general, the resonance width of all the molecules broadens as the amplitude  $G$  of the fast excitation increases. The response curves for  $\text{HF}$  and  $\text{O}_2$  overlap, both in height and width – with the peaks appearing at relatively low values of  $G$ . Their narrow resonance widths suggests slower transitions in and out of their resonant states [80].

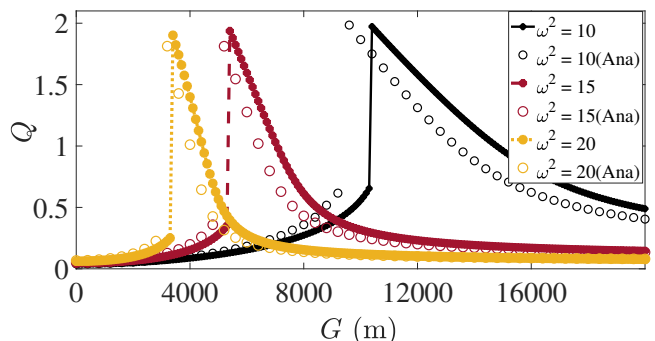


FIG. 5. Dependence of the response amplitude  $Q$  on the amplitude  $G$  of the fast oscillation, for  $\Omega = 70.0$ ,  $d = 0.1$ , and  $F = 0.1$ , for different values of  $\omega^2 = (10, 15, \text{ and } 20)$ , using the parameters for the  $\text{H}_2$  diatomic molecule. The response amplitude  $Q$  computed by the numerical solution of equation (15) in equation (16) is shown by continuous lines, while the markers represent the analytic solution derived from equation (14).

Figure 8 plots the response amplitude  $Q$  against the frequency  $\Omega$  of the high frequency excitation for all of the molecules investigated. For  $\text{CO}$ ,  $\text{N}_2$ , and  $\text{NO}$ , VR occurs at lower values of  $\Omega$ , with relatively decreased resonance widths compared to the other molecules.  $\text{HF}$  and  $\text{O}_2$  exhibit broader widths at higher values of  $\Omega$ , with nearly overlapping response curves and the same resonance frequency for the fast excitation. The  $\text{H}_2$  molecule exhibited the highest response peak, at the highest value of  $\Omega$ , and a broader resonance width. The  $\text{I}_2$  and  $\text{Cl}_2$  molecules exhibited the weakest response to high-frequency excitation.

To unravel the underlying dynamical mechanism associated with the occurrence of VR at distinct parameter

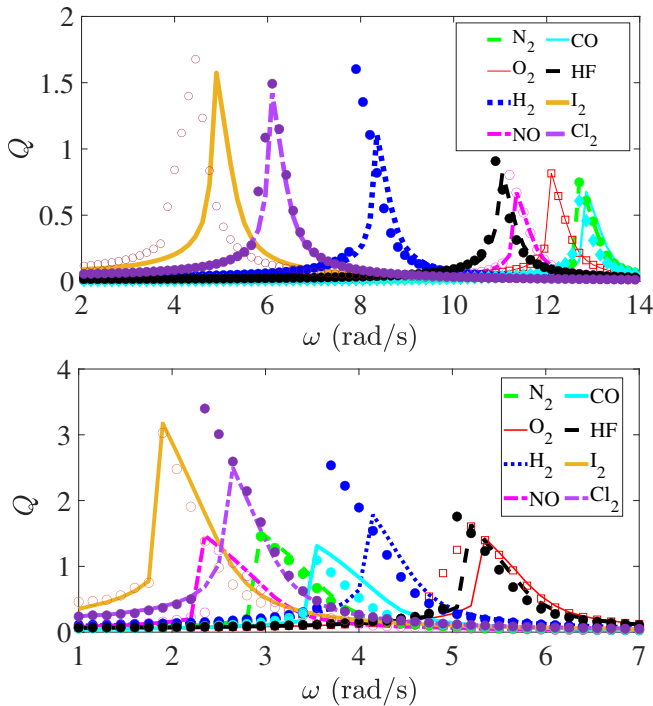


FIG. 6. The low-frequency response-curve for  $F = 0.1$ ,  $d = 0.1$ ,  $\Omega = 70$ , and  $G = 0$  (upper panel) and  $G = 12,000$  (lower panel) for eight different diatomic molecules. The continuous curves represent numerical computations, while the analytic solutions are indicated by marker points.

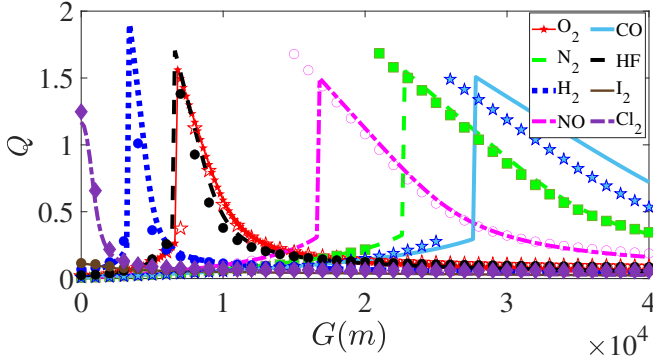


FIG. 7. Dependence of the response amplitude  $Q$  on the fast excitation amplitude  $G$ , with  $F = 0.1$ ,  $d = 0.1$ ,  $\omega = \sqrt{20}$ , and  $\Omega = 70.0$  for eight different diatomic molecules. The continuous curves represent the numerically computed  $Q$ , while the analytic solutions are indicated by marker points.

values of the faster excitation for the non-halogens and heterogeneous halogens, and its non-occurrence for the homogeneous halogens in the same parameter space, we explored the bifurcations of the periodic orbits in the Poincaré surface of section, using the slow motion dynamics around the equilibrium point,  $\chi_x$ , given by Eq. 11. We therefore compute the orbits as a series of points in  $(r, \dot{r})$  phase-space, plotting a single point per cycle of the low-frequency  $\omega$  excitation, in the relevant bifurcation

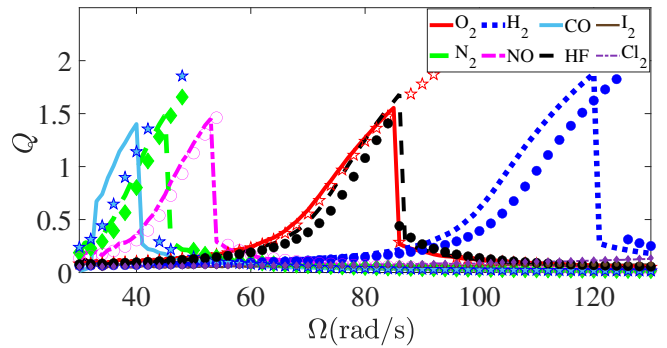


FIG. 8. The high-frequency response curve for  $F = 0.1$ ,  $d = 0.1$ ,  $\omega = \sqrt{20}$ , and  $G = 10,000$  for the eight different diatomic molecules. The continuous curves represent the numerically computed  $Q$ , while the analytic solutions are indicated by marker points.

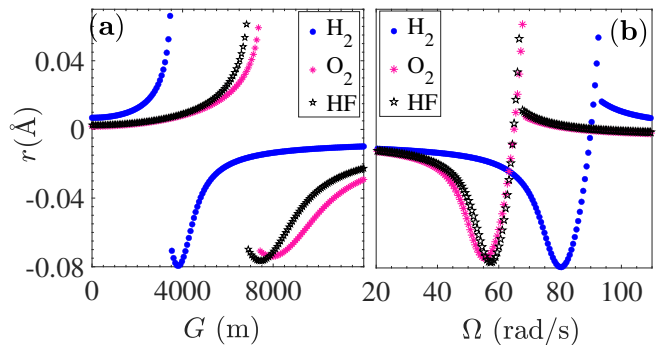


FIG. 9. Bifurcation diagrams of  $r$ , varying the high-frequency forcing parameters  $G$  and  $\Omega$  for  $\text{H}_2$ ,  $\text{O}_2$  and  $\text{HF}$ , with  $F = 0.1$ ,  $d = 0.1$ , and  $\omega = \sqrt{20}$ .

parameter regimes. We choose  $G$  and  $\Omega$  as the bifurcation parameters, as shown in Fig. 9(a) and (b), respectively, for the  $\text{H}_2$ ,  $\text{O}_2$  and  $\text{HF}$  molecules. We find that in both plots, the saddle-node (SN-) bifurcation occurs at exactly the same  $G$  and  $\omega$  values as those at which resonance appeared in Figs. 7 and 8, respectively. Similarly, the bifurcation diagrams for  $\text{NO}$ ,  $\text{CO}$ , and  $\text{N}_2$  are shown in Fig. 10. Again, the SN-bifurcations occur at exactly the same  $G$  and  $\omega$  values as those at which resonance appeared in Figs. 7 and 8, respectively, for these three molecules. For the homogeneous halogens  $\text{I}_2$  and  $\text{Cl}_2$ , the bifurcation structures plotted in Fig. 11 show no evidence of SN-bifurcations, nor of any other form of bifurcation in the parameter space. Rather, the orbit grows exponentially with varying  $G$  and saturates at a  $G$  value above which it attains the quiescent state. On the contrary, with a fixed value of  $G$ , and  $\Omega$  as the bifurcation parameter, the orbit decays exponentially, moving with negative velocity against increasing  $\Omega$ . Thus, the occurrence of SN-bifurcations seems to be associated with the appearance of VR for the non-halogens and heterogeneous halogen studied, and the non-occurrence of SN-bifurcations seems to be associated with the non-appearance of VR

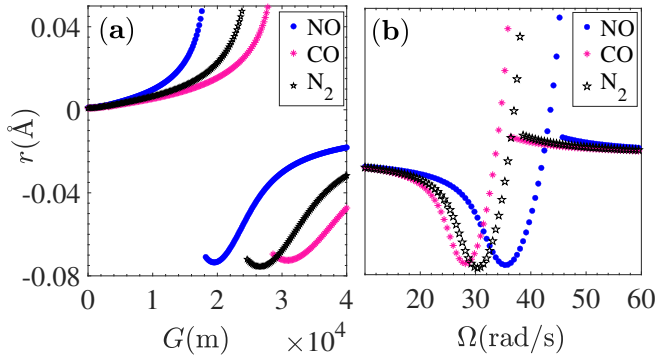


FIG. 10. Bifurcation diagrams of  $r$ , varying the high-frequency forcing parameters  $G$  and  $\Omega$  for NO, CO, and  $N_2$ , with  $F = 0.1$ ,  $d = 0.1$ , and  $\omega = \sqrt{20}$ .

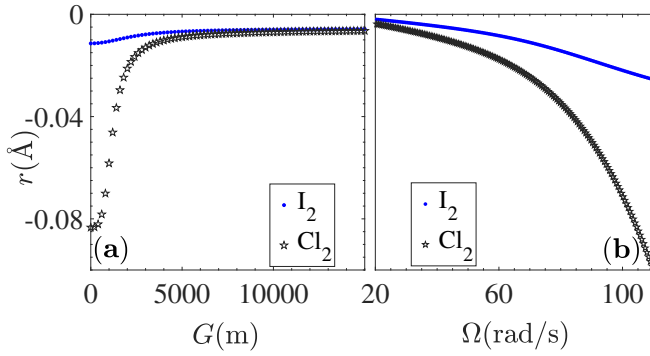


FIG. 11. Bifurcation diagrams of  $r$ , varying the high-frequency forcing parameters  $G$  and  $\Omega$  for  $I_2$ , and  $Cl_2$ , with  $F = 0.1$ ,  $d = 0.1$ , and  $\omega = \sqrt{20}$ .

in the parameter space of the fast excitation component of the homogeneous halogens.

To gain further insights into the transition, we explored the corresponding phase portraits. We present these for five different values of the fast oscillation amplitudes  $G$ , for each of the molecules. In each case, the phase portraits consist of closed periodic orbits within the phase

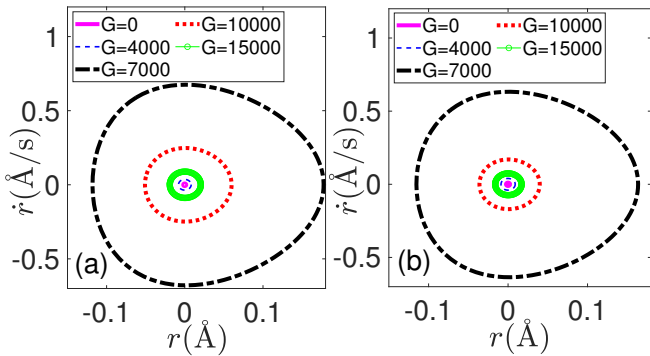


FIG. 12. Phase portraits for  $F = 0.1$ ,  $\omega = \sqrt{20}$ ,  $\Omega = 70.0$ . (a)  $O_2$  diatomic molecule for  $G = 0, 4000, 7000, 10000, 15000$ . (b) HF diatomic molecule for  $G = 0, 2000, 26000, 30000, 40000$ .

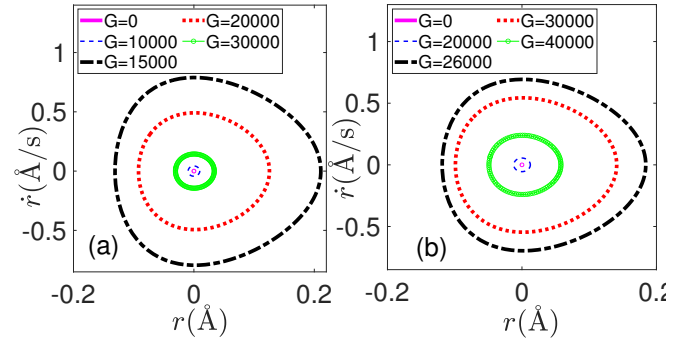


FIG. 13. Phase portraits for  $F = 0.1$ ,  $\omega = \sqrt{20}$ ,  $\Omega = 70.0$ . (a) NO diatomic molecule for  $G = 0, 10000, 15000, 20000, 30000$ . (b) CO diatomic molecule for  $G = 0, 20000, 26000, 30000, 40000$ .

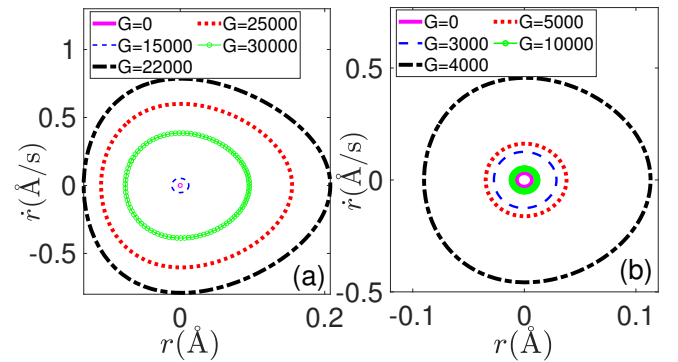


FIG. 14. Phase portraits for  $F = 0.1$ ,  $\omega = \sqrt{20}$ ,  $\Omega = 70.0$ . (a)  $N_2$  diatomic molecule for  $G = 0, 15000, 22000, 25000, 30000$ . (b)  $H_2$  diatomic molecule for  $G = 0, 3000, 4000, 5000, 10000$ .

space, thus signifying repetitive patterns in the vibrational dynamics of all the molecules studied. Figure 12(a) shows the phase space for  $G = 0, 4000, 7000, 10000$ , and 15000 for the  $O_2$  molecule. As the amplitude  $G$  of the fast excitation increases, the phase portrait reveals interesting dynamics exhibited by the  $O_2$  molecule. When

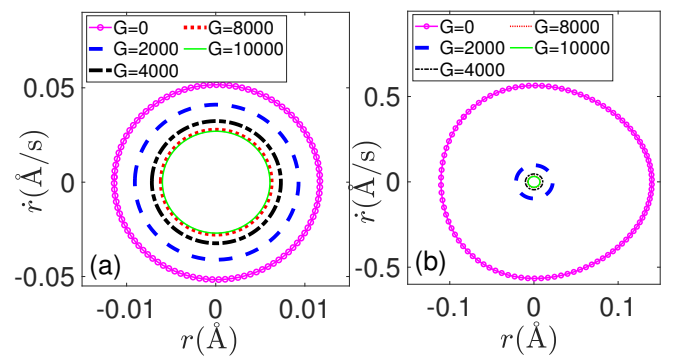


FIG. 15. Phase portraits for  $F = 0.1$ ,  $\omega = \sqrt{20}$ ,  $\Omega = 70.0$ . (a)  $I_2$  diatomic molecule for  $G = 0, 2000, 4000, 8000, 10000$ . (b)  $Cl_2$  diatomic molecule for  $G = 0, 2000, 4000, 8000, 10000$ .

$G = 0$ , the orbits exhibit minimal vibrational motion in a periodic cycle in the close neighbourhood of the zero equilibrium. As  $G$  is increased the periodic orbit expands, indicating an enhanced vibration. At  $G \approx 7000$ , however, the orbit reaches a maximum vibration amplitude. For  $G > 7000$  the orbits begin to shrink again and, at  $G = 10000$  and  $15000$ , a change in the periodic behavior occurs. Thus increasing the fast excitation amplitude beyond  $G = 10000$  does not lead to a corresponding increase in the amplitude of vibrational motion. Instead, the molecular vibration saturates.

Figure 12(b) displays the phase portrait of an HF molecule for  $G = 0, 4000, 7000, 10000,$  and  $15000$ . The orbit behaves in similar manner to that of  $O_2$ , except that the maximum vibrational response for HF molecule occurs at  $G = 7000$ . At  $G = 10000, 15000$ , the orbit attains its saturation point above which further increase in the amplitude does not lead to the expansion of the molecular orbit; rather it shrinks it.

Comparable behaviour was found for the other non-halogen molecules. Figure 13 shows the phase portraits for, respectively: (a) the NO molecule at  $G = 0, 10000, 15000, 20000,$  and  $30000$ ; and (b) the CO molecule at  $G = 0, 20000, 26000, 30000,$  and  $40000$ . The maximum vibrational responses for the two molecules occur at  $G = 15000$  and  $G = 26000$ .

Figure 14 shows the phase portraits: for (a)  $N_2$  at  $G = 0, 15000, 22000, 25000,$  and  $30000$ ; and for (b)  $H_2$  at  $G = 0, 3000, 4000, 5000,$  and  $10000$ . For the  $N_2$  molecule, the orbit experiences a maximum vibrational state when the fast excitation amplitude is  $G = 22000$ , and as the amplitude is further increased, the orbits contracts progressively. Similarly, beyond the maximum vibrational state at  $G = 4000$ , the phase space plot for the  $H_2$  molecule shows that the orbit no longer expands but contracts to lower value of the amplitude where  $G = 3000$  and close to orbit when  $G = 0$ , as the  $H_f$  amplitude is further increased to  $G = 10000$ .

The phase portraits for  $I_2$  and  $Cl_2$  in Fig. 15(a) and (b) display distinctly different behaviour compared to that of the other diatomic molecules studied, whose results are presented in Figs. 12 – 14. Both  $I_2$  and  $Cl_2$ , shows their maximum vibrational response to be at  $G = 0$ , with monotonically decreasing responses with increasing excitation amplitude from  $G = 0$  through  $G = 2000, 4000, 8000,$  and  $10000$ , respectively.

To illuminate broader features of the response in the parameter spaces of the eight diatomic molecules, we further explored three-dimensional plots in two-parameter spaces of the biharmonic field. Figure 16 shows 3-D plots of the response  $Q$  in the parameter space of the high frequency signal for all the eight diatomic molecules studied. We thus explore the fast excitation parameter-space for which each of the diatomic molecules exhibits VR relative to Figures 7 and 8. The plots confirmed the evidence for just a single resonance peak for each molecule, in agreement with Figures 7 and Fig. 8. Moreover, it is clear that high frequency parameter spaces of the molecules

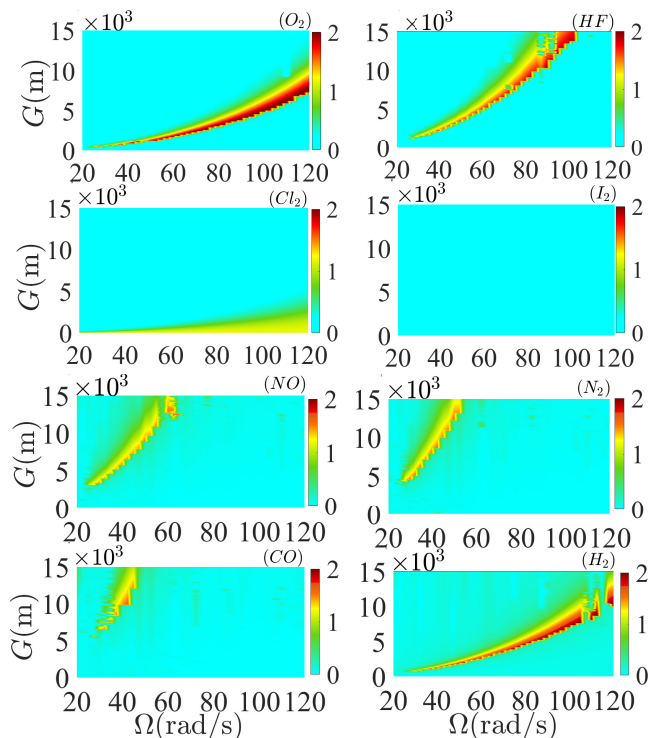


FIG. 16. Three-dimensional plots showing the dependence of the response amplitude  $Q$  on the parameters  $(\Omega, G)$  of the high frequency force parameters, for  $F = 0.1, d = 0.1,$  and  $\omega = \sqrt{20}$ . (a)  $O_2$ , (b) HF, (c)  $Cl_2$ , (d)  $I_2$ , (e) NO, (f)  $N_2$ , (g) CO, and (h)  $H_2$  diatomic molecules, respectively. The molecular responses to the high-frequency driving force are shaded with increasing color density, from cyan(gray) to red(black) color, where the cyan(gray) color denotes weak/moderate response and red (black) denotes the parameter regime for maximum response.

for which resonance occurs differ significantly between each other. For instance, in Fig. 16 while VR will not occur for  $G > 10000$  in  $O_2$ , it will occur for  $G > 10000$  in HF. On the other hand, for  $\Omega > 100$ , VR will occur in  $O_2$ , but will not occur in HF. In contrast to the behavior of these two molecules, the scenario is again, completely different for  $Cl_2$  and  $I_2$ . While there is clearly no evidence of VR in  $I_2$ , VR does occur within the weak amplitude region of the high frequency driving force, with its window increasing with  $\Omega$  and with  $G$ . The observed pattern differs from behavior exhibited by NO,  $N_2$  and CO, but the response amplitude of  $H_2$  appears to increase proportionally with increase in the parameters of the fast component of the bichromatic excitation. This is consistent with the dependence of  $Q$  on  $\Omega$  for different diatomic molecule as shown in Fig. 8 and also with the bifurcation structures shown in Fig. 10.

## V. CONCLUDING REMARKS

Diatomic molecules are encountered in numerous natural and industrial processes, including but not limited to combustion, atmospheric chemistry, water-cooled nuclear reactors, and laser spectroscopy. Their ubiquitous nature has made them a subject of interdisciplinary interest and close scientific study for decades [44, 48, 49, 59, 60]. We discuss above vibrational resonance in a classical diatomic model, with parameters matching eight diatomic molecules excited by bi-harmonic fields in the shifted Tietz-Wei molecular potential. Our theoretical and numerical study has revealed evidence that VR – the amplification of the response of the molecules to a low-frequency field when also acted upon by a high-frequency field – will occur in a molecule at distinct parameter values of the high frequency field. The VR arises where SN-bifurcation takes place, and does not occur in the absence of SN-bifurcation. Specifically, with the fast excitation amplitude  $G$  chosen as the bifurcation parameter, six of the diatomic molecules considered exhibited single resonance peaks at different values of  $G$ , while the homogeneous halogens ( $I_2$  and  $Cl_2$ ) exhibited no resonance within the simulated  $G$ -parameter space. Similarly, with the fast signal frequency ( $\Omega$ ) treated as the bifurcation parameter,  $I_2$  showed no resonance, and  $Cl_2$  showed a weak response; while each of the non-halogens  $H_2$ ,  $O_2$ ,  $HF$ ,  $CO$ ,  $NO$  and  $N_2$  exhibited single resonance peaks. The phase portraits showed that the orbits for all the non-halogen molecules expanded progressively as  $G$  increased above the SN-bifurcation value where VR occurred, the orbits for  $I_2$  and  $Cl_2$  did not expand beyond  $G = 0$ , where the primary resonance exists. We conjecture that the weak response of the homogeneous halo-

gens, linked to the nonoccurrence of SN-bifurcation, may also be attributable to their heavier masses compared to those of the non-halogens studied.

Our results provide a novel approach for exploring and elucidating the rich properties and vibrational dynamics of homogeneous and heterogeneous diatomic molecules, with potential implications for several fields, including chemical kinetics and molecular spectroscopy. Beyond advancing existing knowledge of VR and diatomic molecules, this work motivates future experimental studies aimed at exploring the unique properties and coherent control of vibrational dynamics in molecular systems. The application of the theoretical method has established that the observed distinct complex behaviours of diatomic molecules in the sTW potential can also be used to predict the behaviour of other gaseous diatomic molecules, such as  $CsO$ ,  $CsF$ , and  $CsCl$  [56], and perhaps more broadly, dimers and polyatomic molecules. Perhaps also taking account of some recently proposed shifted-potential functions, the study of VR could advance knowledge of molecular properties, including those of polyatomic molecules, for which appropriate molecular potentials from fitting the spectroscopic parameter values are now available.

### DATA

No new data were recorded or created in the course of this research.

### FUNDING

The work was supported by the Engineering and Physical Sciences Research Council, United Kingdom (grant number EP/X004597/1)

---

Appendix: Appendix1

---

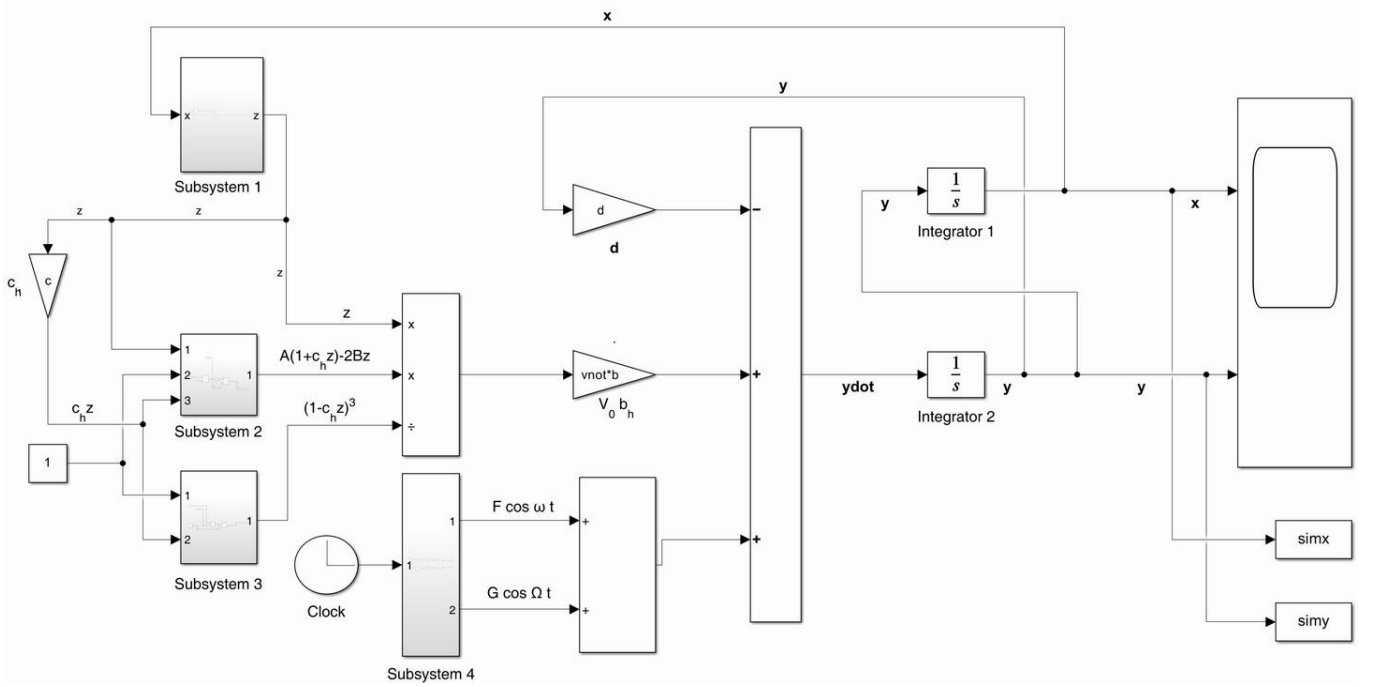


FIG. 17. A block diagram of the MATLAB-Simulink-designed dual-frequency driven shifted Tietz-Wei oscillator (Eq. 15) that describes the dynamics of bichromatically excited diatomic molecules. Subsystem 1 of Fig. 17 is a Simulink subsystem designed to take  $x$  as its only input and compute  $z = e^{-b_h(x-r_e)}$ . Subsystem 2 in Fig. 17 takes  $z$ ,  $1$ , and  $c_h z$  as inputs 1, 2, and 3, respectively. It is made up of product and sum blocks that result in the output  $A(1+c_h z)-2Bz$ . Subsystem 3 takes  $1$  and  $c_h z$  as inputs and consists of a sum and power function block that computes  $(1-c_h z)^3$ . Subsystem 4 is a time-function block that takes time as an input and outputs the sinusoidal functions  $F \cos \omega t$  and  $G \cos \Omega t$ . The outputs of the Subsystems 1-3 were combined with a product block, which serves as the input for the gain block, which amplifies the input signal by the factor  $V_0 b_h$ . A sum block was used to feed the appropriate signals to the two integrator blocks, resulting in the desired solutions  $x$  and  $y$  as seen through a connected scope. Simx and Simy are two interconnected data logging blocks.

- 
- [1] R.V. and V. Letokhov, Multiple photon infrared laser photochemistry, in *Chemical and Biochemical Applications of Lasers*, Vol. III, edited by C. Moore (Academic Press, New York, 1977) Chap. 2, pp. 167–314.
- [2] J. Jarvis, Stephen, D. J. Wineland, and H. Hellwig, Two-frequency excitation for the Ramsey separated oscillatory field method, *J. Appl. Phys.* **48**, 5336 (1977).
- [3] J. Stine and D. Noid, Classical treatment of the dissociation of hydrogen fluoride with one and two infrared lasers, *Opt. Commun.* **31**, 161 (1979).
- [4] J. Stine and D. Noid, The effect of laser polarization on the two-laser excitation of a diatomic molecule, *Chem. Phys. Lett.* **77**, 287 (1981).
- [5] D. Noid and J. Stine, The excitation of HF by two polarized lasers and the effect of laser power, *Opt. Commun.* **37**, 187 (1981).
- [6] M. H. Nayfeh, K. King, G. B. Hillard, I. S. Shahin, and A. H. Nayfeh, Intensity-induced quenching of absorption of diatomic molecules in two near-resonance laser fields, *Phys. Rev. A* **26**, 1988 (1982).
- [7] M. H. Nayfeh, K. K. King, and J. Shobaki, Effect of dephasing on the molecular absorption in a two-frequency field, *J. Appl. Phys.* **56**, 1944 (1984).
- [8] A. Datta, S. S. Bhattacharyya, S. Lee, and B. Kim, Atomic and molecular stabilization in two-frequency laser fields, *J. Chem. Phys.* **119**, 2083 (2003).
- [9] V. Constantoudis and C. A. Nicolaides, Stabilization and relative phase effects in a dichromatically driven diatomic Morse molecule: Interpretation based on nonlinear classical dynamics, *J. Chem. Phys.* **122**, 084118 (2005).
- [10] S. Huang, C. Chandre, and T. Uzer, Bifurcations as dissociation mechanism in bichromatically driven diatomic molecules, *J. Chem. Phys.* **128**, 174105 (2008).
- [11] A. Datta, Phase control in photodissociation of  $H_2$  using pairs  $(\omega, \omega)$  of chirped laser fields, *Eur. Phys. J. D* **76**, 1 (2022).
- [12] U. Feudel, S. Kuznetsov, and A. Pikovsky, *Strange Nonchaotic Attractors: Dynamics between Order and Chaos in Quasiperiodically Forced Systems*, Nonlinear Science A, Vol. 56 (World Scientific Series, Singapore, 2002).
- [13] X. Han, Y. Liu, Q. Bi, and J. Kurths, Frequency-truncation fast-slow analysis for parametrically and externally excited systems with two slow incommensurate excitation frequencies, *Commun. Nonlin. Sci. Numer. Simulat.* **72**, 16 (2019).
- [14] K. S. Oyeleke, O. I. Olusola, O. T. Kolebaje, U. E. Vincent, A. B. Adeyoye, and P. V. E. McClintock, Novel bursting oscillations in a nonlinear gyroscope oscillator, *Phys. Scr.* **97**, 085211 (2022).
- [15] Z. Chen and F. Chen, Bifurcation behaviors and bursting regimes of a piezoelectric buckled beam harvester under fast-slow excitation, *Nonlinear Dyn.* **111**, 4121–4139 (2023).
- [16] P. S. Landa and P. V. E. McClintock, Vibrational resonance, *J. Phys. A: Math. Gen.* **33**, L433 (2000).
- [17] S. Rajasekar and M. A. F. Sanjuán, *Nonlinear Resonances, Springer Series in Synergetics* (Springer, Switzerland, 2016).
- [18] U. E. Vincent, P. V. E. McClintock, I. A. Khovanov, and S. Rajasekar (Eds.), Vibrational and stochastic resonances in driven nonlinear systems, *Phil. Trans. R. Soc. A* **379**, 20200226 (2021).
- [19] U. E. Vincent, P. V. E. McClintock, I. A. Khovanov, and S. Rajasekar (Eds.), Vibrational and stochastic resonance in driven nonlinear systems - part two, *Phil. Trans. R. Soc. A* **379**, 20200226 (2021).
- [20] J. Yang, S. Rajasekar, and M. A. Sanjuán, Vibrational resonance: A review, *Phys. Rep.* **1067**, 1 (2024).
- [21] U. E. Vincent, T. O. Roy-Layinde, O. O. Popoola, P. O. Adesina, and P. V. E. McClintock, Vibrational resonance in an oscillator with an asymmetrical deformable potential, *Phys. Rev. E* **98**, 062203 (2018).
- [22] S. J. Gilbert, L. D. Barnes, J. P. Sullivan, and C. M. Surko, Vibrational-Resonance Enhancement of Positron Annihilation in Molecules, *Phys. Rev. Lett.* **88**, 043201 (2002).
- [23] G. F. Gribakin, J. A. Young, and C. M. Surko, Positron-molecule interactions: Resonant attachment, annihilation, and bound states, *Rev. Mod. Phys.* **82**, 2557 (2010).
- [24] G. F. Gribakin and C. M. R. Lee, Positron Annihilation in Molecules by Capture into Vibrational Feshbach Resonances of Infrared-Active Modes, *Phys. Rev. Lett.* **97**, 193201 (2006).
- [25] G. F. Gribakin, J. F. Stanton, J. R. Danielson, M. R. Natisin, and C. M. Surko, Mode coupling and multi-quantum vibrational excitations in Feshbach-resonant positron annihilation in molecules, *Phys. Rev. A* **96**, 062709 (2017).
- [26] Z. Cheong, D. Stevens, and J. P. Sullivan, Positron resonances in vibrational excitation, *Phys. Rev. A* **109**, 042812 (2024).
- [27] T. Roy-Layinde, U. Vincent, S. A. Abolade, O. O. Popoola, J. A. Laoye, and P. V. E. McClintock, Vibrational resonances in driven oscillators with position-dependent mass, *Phil. Trans. Roy. Soc. A* **379**, 20200227 (2021).
- [28] G. Madiot, S. Barbay, and R. Braive, Vibrational resonance amplification in a Thermo-Optic Optomechanical Nanocavity, *Nano Lett.* **21**, 8311 (2022).
- [29] V. N. Chizhevsky and M. V. Lakhmitski, Improvement of signal propagation in the optoelectronic artificial spiking neuron by vibrational resonance, *Phys. Rev. E* **109**, 014211 (2024).
- [30] M. I. Dykman, D. G. Luchinsky, R. Mannella, P. V. E. McClintock, N. D. Stein, and N. G. Stocks, Stochastic resonance in perspective, *Nuovo Cimento D* **17**, 661 (1995).
- [31] J. Casado-Pascual, J. Gómez-Ordóñez, and M. Morillo, Stochastic resonance: theory and numerics., *Chaos* **15**, 26115 (2005).
- [32] M. Gitterman, Bistable oscillator driven by two periodic fields, *J. of Phys. A: Math. & Gen.* **34**, L355 (2001).
- [33] I. I. Blekhan and P. S. Landa, Conjugate resonances and bifurcations in nonlinear systems under biharmonic excitation, *Intern. J. Non-Lin. Mech.* **39**, 421 (2004).
- [34] J. P. Baltanás, L. López, I. I. Blekhan, P. S. Landa, A. Zaikin, J. Kurths, and M. A. F. Sanjuán, Experimental evidence, numerics, and theory of vibrational resonance in bistable systems, *Phys. Rev. E* **67**, 066119 (2003).
- [35] V. N. Chizhevsky, E. Smeu, and G. Giacomelli, Experimental evidence of vibrational resonance in an optical

- system, *Phys. Rev. Lett.* **91**, 220602 (2003).
- [36] V. N. Chizhevsky, Vibrational higher-order resonances in an overdamped bistable system with biharmonic excitation, *Phys. Rev. E* **90**, 042924 (2014).
- [37] V. N. Chizhevsky, Experimental evidence of vibrational resonance in a multistable system, *Phys. Rev. E* **89**, 062914 (2014).
- [38] V. N. Chizhevsky, Noise-induced suppression of nonlinear distortions in a bistable system with biharmonic excitation in vibrational resonance, *Phys. Rev. E* **92**, 032902 (2015).
- [39] W. Knop and W. Lauterborn, Bifurcation structure of the classical Morse oscillator, *J. Chem. Phys.* **93**, 3950 (1990).
- [40] Z. Jing, J. Deng, and J. Yang, Bifurcations of periodic orbits and chaos in damped and driven Morse oscillator, *Chaos Soliton Fract.* **35**, 486 (2008).
- [41] K. Abirami, S. Rajasekar, and M. A. F. Sanjuán, Vibrational resonance in the morse oscillator, *Pramana* **81**, 127 (2013).
- [42] J. A. Kunc and F. J. Gordillo-Vázquez, Rotational-vibrational levels of diatomic molecules represented by the Tietz-Hua rotating oscillator, *J. Phys. Chem. A* **101**, 1595 (1997).
- [43] P. M. Morse, Diatomic molecules according to the wave mechanics. II. Vibrational Levels, *Phys. Rev.* **34**, 57 (1929).
- [44] J. P. Araújo and M. Y. Ballester, A comparative review of 50 analytical representation of potential energy interaction for diatomic systems: 100 years of history, *Int J Quantum Chem.* **15**, e26808. (2021).
- [45] B. J. Falaye, S. M. Ikhdaïr, and M. Hamzavi, Shifted Tietz-Wei oscillator for simulating the atomic interaction in diatomic molecules, *J. Theor. Appl. Phys.* **9**, 151 (2015).
- [46] W. Hua, Four-parameter exactly solvable potential for diatomic molecules, *Phys. Rev. A* **42**, 2524 (1990).
- [47] O. I. Olusola, O. P. Shomotun, U. E. Vincent, and P. V. E. McClintock, Quantum vibrational resonance in a dual-frequency driven Tietz-Hua quantum well, *Phys. Rev. E* **101**, 052216 (2020).
- [48] Y. P. Varshni, Comparative study of potential energy functions for diatomic molecules, *Rev. Mod. Phys.* **29**, 664 (1957).
- [49] D. Steele, E. R. Lippincott, and J. T. Vanderslice, Comparative study of empirical internuclear potential functions, *Rev. Mod. Phys.* **34**, 239 (1962).
- [50] M. S. Abdelmonem, A. Abdel-Hady, and I. Nasser, Dealing with the shifted and inverted Tietz-Hua oscillator potential using the J-matrix method, *Inter. J. Quan. Chem.* **116**, 897 (2016).
- [51] U. S. Okorie, E. E. Ibekwe, M. C. Onyeaju, and A. N. Ikot, Solutions of the Dirac and Schrödinger equations with shifted Tietz potential, *Eur. Phys. J. Plus* **133**, 433 (2018).
- [52] C. A. Onate, M. C. Onyeaju, E. E. Ituen, A. N. Ikot, O. Ebomwonyi, J. O. Okoro, and K. O. Dopamu, Eigen-solutions, Shannon entropy and information energy for modified Tietz-Hua potential, *Indian J. Phys.* **92**, 487 (2018).
- [53] A. N. Ikot, W. Azogor, U. S. Okorie, F. E. Bazuaye, M. C. Onyeaju, C. A. Onate, and E. O. Chukwuocha, Exact and Poisson summation thermodynamic properties for diatomic molecules with shifted Tietz potential, *Indian J. Phys.* **93**, 1171 (2019).
- [54] R. Horchani and H. Jelassi, Comments on the paper “Exact and Poisson summation thermodynamic properties for diatomic molecules with shifted Tietz potential”, *Indian J. Phys.* **96**, 373 (2022).
- [55] U. S. Okorie, A. N. Ikot, G. J. Rampho, M. C. Onyeaju, M. U. Ibezim-Ezeani, and A. Abdel-Aty, Bound and scattering states of the Klein-Gordon equation for shifted Tietz-Wei potential with applications to diatomic molecules, *Mol. Phys.* **119**, 1171 (2021).
- [56] R. Horchani, S. Shafii, H. Friha, and H. Jelassi, A straightforward model for molar enthalpy prediction of CsO, CsF, and CsCl molecules via shifted Tietz-Wei potential, *Int. J. Thermophys.* **42**, 84 (2021).
- [57] R. Horchani and H. Jelassi, A four-parameters model for molar entropy calculation of diatomic molecules via shifted Tietz-Wei potential, *Chem. Phys. Lett.* **753**, 137583 (2020).
- [58] J. A. Kerr, K. P. Huber, and G. Herzberg, Molecular spectra and molecular structure: IV constants of diatomic molecules, *Anal. Chim. Acta* **144**, 298 (1982).
- [59] S. Svanberg, *Atomic and Molecular Spectroscopy: Basic Aspects and Practical Applications*, 4th ed. (Springer Berlin, Heidelberg, 1992).
- [60] C. G. Parigger, Atomic and molecular emissions in laser-induced breakdown spectroscopy, *Spectrochim. Acta Part B At. Spectrosc.* **79-80**, 4 (2013).
- [61] N. J. English and C. J. Waldron, Perspectives on external electric fields in molecular simulation: progress, prospects and challenges, *Phys. Chem. Chem. Phys.* **17**, 12407 (2015).
- [62] B. J. Falaye, G.-H. Sun, R. Silva-Ortigoza, and S.-H. Dong, Hydrogen atom in a quantum plasma environment under the influence of aharonov-bohm flux and electric and magnetic fields, *Phys. Rev. E* **93**, 053201 (2016).
- [63] C. O. Edet and A. N. Ikot, Analysis of the impact of external fields on the energy spectra and thermo-magnetic properties of n 2, i 2, co, no and hcl diatomic molecules, *Mol. Phys.* **119**, e1957170 (2021).
- [64] M. Bansal, V. Kumar, Sahil, S. Bhardwaj, R. M. Singh, and F. Chand, Investigation of linear and nonlinear optical properties in quantum dots: Influence of magnetic and ab flux fields, *Physica B: Cond. Matt.* **676**, 415654 (2024).
- [65] F. Urgan, J. Martínez-Orozco, R. Restrepo, M. Mora-Ramos, E. Kasapoglu, and C. Duque, Nonlinear optical rectification and second-harmonic generation in a semi-parabolic quantum well under intense laser field: Effects of electric and magnetic fields, *Superlattices and Microstruct.* **81**, 26 (2015).
- [66] F. Urgan, Effects of applied electric and magnetic fields on the nonlinear optical rectification and second-harmonic generation in a graded quantum well under intense laser field, *Eur. Phys. J. B* **90**, 1 (2017).
- [67] U. Yesilgul, H. Sari, F. Urgan, J. Martínez-Orozco, R. Restrepo, M. Mora-Ramos, C. Duque, and I. Sökmen, Effects of electromagnetic fields on the nonlinear optical properties of asymmetric double quantum well under intense laser field, *Chem. Phys.* **485-486**, 81 (2017).
- [68] N. J. English and C. Waldron, Perspectives on external electric fields in molecular simulation: progress, prospects and challenges, *Phys. Chem. Chem. Phys.* **17**, 12407 (2015).
- [69] J. F. Ogilvie, A general potential energy function for di-

- atomic molecules, *Proc. Roy. Soc. A* **378**, 287 (1981).
- [70] B. J. Falaye, S. M. Ikhdaïr, and M. Hamzavi, Spectroscopic study of some diatomic molecules via the proper quantization rule, *J. Math. Chem.* **53**, 1325 (2015).
- [71] J. A. Kunc and F. A. Gordillo-Vazquez, Rotational-vibrational levels of diatomic molecules represented by the Tietz-Hua rotating oscillator, *J. Phys. Chem. A* **101**, 1595 (1997).
- [72] B. J. Falaye, K. J. Oyewumi, S. M. Ikhdaïr, and M. Hamzavi, Eigensolution techniques, their applications and Fisher's information entropy of the Tietz-Wei diatomic molecular model, *Phys. Scr.* **89**, 115204 (2014).
- [73] M. J. Idrissi, A. Fedoul, and S. Sayouri, Systematic approach to compute the vibrational energy levels of diatomic molecules, *J. App. Math. Phys.* **8**, 2463 (2020).
- [74] O. T. Kolebaje, U. E. Vincent, B. E. Benyeogor, and P. V. E. McClintock, Effect of a modulated acoustic field on the dynamics of a vibrating charged bubble, *Ultrasonics* **135**, 107110 (2023).
- [75] C. H. Miwadinou, A. V. Monwanou, L. A. Hinvi, V. K. Tamba, A. A. Koukémèdji, and J. B. Chabi Orou, Nonlinear oscillations of nonlinear damping gyros: Resonances, hysteresis and multistability, *Int. J. Bifurc. Chaos* **30**, 2050203 (2020).
- [76] A. Chudzik, P. Perlikowski, A. Stefanski, and T. Kapitaniak, Multistability and rare attractors in van der Pol-Duffing oscillator, *Int. J. Bifurc. Chaos* **21**, 1907 (2011).
- [77] R. D. Artuso and G. W. Bryant, Strongly coupled quantum dot-metal nanoparticle systems: Exciton-induced transparency, discontinuous response, and suppression as driven quantum oscillator effects, *Phys. Rev. B* **82**, 195419 (2010).
- [78] X. Wei, L. Ruihong, and L. Shuang, Resonance and bifurcation in a nonlinear Duffing system with cubic coupled terms, *Nonlinear Dynamics* **46**, 211 (2006).
- [79] S. Rajasekar and K. Murali, Resonance behaviour and jump phenomenon in a two coupled Duffing-van der Pol oscillators, *Chaos, Solitons & Fractals* **19**, 925 (2004).
- [80] S. Hollerith and J. Zeiher, Rydberg macrodimers: Diatomic molecules on the micrometer scale., *J. Phys. Chem. A* **127**, 3925 (2023).